INSTITUTE OF PHYSICS PUBLISHING PHYSICS IN MEDICINE AND BIOLOGY

Phys. Med. Biol. **49** (2004) 1183–1201 PII: S0031-9155(04)76424-6

Optical measurements of absorption changes in two-layered diffusive media

Francesco Fabbri[1], **Angelo Sassaroli**[1], **Michael E Henry**[2] **and Sergio Fantini**[1]

[1] Department of Biomedical Engineering, Bioengineering Center, Tufts University, 4 Colby Street, Medford, MA 02155, USA
[2] McLean Hospital and Department of Psychiatry, Harvard Medical School, 115 Mill Street, Belmont, MA 02478, USA

Received 18 October 2003
Published 18 March 2004
Online at stacks.iop.org/PMB/49/1183 (DOI: 10.1088/0031-9155/49/7/007)

Abstract

We have used Monte Carlo simulations for a two-layered diffusive medium to investigate the effect of a superficial layer on the measurement of absorption variations from optical diffuse reflectance data processed by using: (a) a multidistance, frequency-domain method based on diffusion theory for a semi-infinite homogeneous medium; (b) a differential-pathlength-factor method based on a modified Lambert–Beer law for a homogeneous medium and (c) a two-distance, partial-pathlength method based on a modified Lambert–Beer law for a two-layered medium. Methods (a) and (b) lead to a single value for the absorption variation, whereas method (c) yields absorption variations for each layer. In the simulations, the optical coefficients of the medium were representative of those of biological tissue in the near-infrared. The thickness of the first layer was in the range 0.3–1.4 cm, and the source–detector distances were in the range 1–5 cm, which is typical of near-infrared diffuse reflectance measurements in tissue. The simulations have shown that (1) method (a) is mostly sensitive to absorption changes in the underlying layer, provided that the thickness of the superficial layer is ∼0.6 cm or less; (2) method (b) is significantly affected by absorption changes in the superficial layer and (3) method (c) yields the absorption changes for both layers with a relatively good accuracy of ∼4% for the superficial layer and ∼10% for the underlying layer (provided that the absorption changes are less than 20–30% of the baseline value). We have applied all three methods of data analysis to near-infrared data collected on the forehead of a human subject during electroconvulsive therapy. Our results suggest that the multidistance method (a) and the two-distance partial-pathlength method (c) may better decouple the contributions to the optical signals that originate in deeper tissue (brain) from those that originate in more superficial tissue layers.

1. Introduction

Near-infrared diffuse reflectance has been used *in vivo* to measure absolute and relative concentrations of endogenous chromophores (for example, haemoglobin, water, lipids and cytochrome oxidase) and exogenous dyes in biological tissue (*Handbook of Optical Biomedical Diagnostics* 2002). Near-infrared light can penetrate several centimetres inside biological tissue (Jöbsis 1977), and is transmitted through skin and bones (Gratton *et al* 1994, 1997). For this reason, near-infrared spectroscopy (NIRS) has been used on human subjects to measure the concentration and oxygen saturation of haemoglobin in brain, breast, muscles, etc (Ferrari *et al* 1997, Delpy and Cope 1997, Villringer and Chance 1997). In these applications, reflectance measurements of continuous, pulsed or intensity-modulated light are employed to measure the absolute or relative value of the absorption coefficient (μ_a) of the investigated tissue; μ_a and its temporal variations are associated with concentrations of tissue chromophores and with their temporal changes, respectively. The measurement of μ_a using reflectance data requires a model for light propagation inside tissue. A common approach in NIRS studies of biological tissue is based on the diffusion equation with semi-infinite boundary conditions (Patterson *et al* 1989, Haskell *et al* 1994, Fantini *et al* 1994); an alternative approach for continuous wave (CW) NIRS is based on a modified Lambert–Beer law (Matcher *et al* 1993). These models often assume that the investigated tissue is homogeneous. However, even at a macroscopic level, many tissues present a layered structure (for example, skin, adipose layer and muscle in the case of limbs; and scalp, skull, cerebrospinal fluid, dura and brain in the case of the head). The heterogeneity of the tissue introduces an ambiguity in the meaning of the single absorption measurement obtained from models that assume a homogeneous medium. A discussion about the accuracy of the absolute value of the absorption coefficient retrieved by using a homogeneous-medium model to analyse *in vivo* data can be found in Weersink *et al* (1997). Homogeneous-medium models are widely used in NIRS even in the strongly heterogeneous case of the human head to measure spatial and temporal changes in the cerebral oxygenation and concentration of haemoglobin (Gopinath *et al* 1993, Meek *et al* 1995, Maki *et al* 1995, Obrig *et al* 2000, Wolf *et al* 2002). More accurate models of the human head have been presented in the literature (Okada *et al* 1997); however, these models have not yet found widespread use because their application usually requires long computational times and, most preferably, *a priori* estimates of geometrical and optical properties of the subject's head that are not always available. Examples of applications of such inhomogeneous models for the analysis of near-infrared data *in vivo* can be found in Bluestone *et al* (2001) and Hillman *et al* (2001). The homogeneous medium assumption applied to the irregular and multilayered structure of the human head may lead to significant errors that are often hard to quantify; in many practical applications, the temporal variations of the absorption measured on a subject's head are just qualitatively, and not quantitatively, associated with changes (increases or decreases) in chromophore concentrations in brain tissue. Under these conditions it would be important to be able to decouple the contributions of the cerebral and extracerebral tissues to the optical data, because temporal changes of μ_a that occur in the brain can be overlapped to concurrent absorption variations localized in the more superficial, extracerebral layers (for example, the scalp or a muscle layer).

In this work, we have used a two-layered medium model to investigate the effect of concurrent absorption changes in the two layers on NIRS reflectance data. We have used Monte Carlo simulations to calculate intensity (dc), amplitude (ac) and phase data for the case of an intensity-modulated pencil beam signal that is incident on a two-layered medium and is detected at several distances from the incidence point. In the simulations, the optical properties of the medium and the thickness of the top layer were chosen to mimic typical cases

of NIRS tissue studies. The distances between illumination and detection points (1.0–5.0 cm) represent typical source–detector distances employed in diffuse reflectance measurements. The absorption variations in the two layers induce changes in ac, dc and phase data that are simulated with the Monte Carlo code. These ac, dc and phase data are translated into absorption changes by applying three methods of data analysis: (a) a multidistance, frequency-domain method based on the diffusion theory (Wolf *et al* 2002); (b) a differential pathlength factor (dpf) method based on a modified Lambert–Beer law (Gopinath *et al* 1993, Meek *et al* 1995, Maki *et al* 1995, Obrig *et al* 2000) and (c) an extension of the modified Lambert–Beer law to heterogeneous media by introducing partial pathlengths (Hiraoka *et al* 1993) and data at two source–detector separations. The third method allows for the determination of individual changes in the absorption coefficients of the two layers, whereas the first two methods yield a single absorption coefficient change to which we refer as an effective absorption change. This study is aimed at:

(1) investigating the relationship between the effective absorption change (measured with the multidistance, frequency-domain method (a) and with the differential pathlength factor method (b)) and the actual absorption changes in the individual layers,
(2) assessing the effectiveness of the partial-pathlength method (c) in two-layered media.

As an example of the insight provided by this study in the analysis of *in vivo* data, we compare the results of methods (a), (b) and (c) as applied to near-infrared data collected on the forehead of a human subject during electro-convulsive therapy (ECT) (Fabbri *et al* 2003).

2. Materials and methods

2.1. Monte Carlo simulations

The results shown in this work were obtained with a direct frequency-domain Monte Carlo (MC) code. This code has been described in detail by Testorf *et al* (1999) and its results have been compared with those of another frequency-domain Monte Carlo code proposed earlier (Yaroslavsky *et al* 1995, 1997). Our MC code was implemented for a two-layered diffusive slab; the first (top) layer had a finite thickness (s_1), whereas the second layer extended infinitely and there are no lateral boundaries. In all the simulations shown in this work, the refractive index mismatch at the outer surface of the medium was set to 1.4. We have chosen several values of s_1 (in the range 0.3–1.4 cm) and optical properties of the two layers to simulate various biological tissues. Furthermore, we have introduced independent variations in the absorption coefficients of the two layers to simulate the effect of concurrent temporal changes in the concentration of chromophores in the two layers. We introduce the following symbols: μ'_{s1} and μ'_{s2} indicate the reduced scattering coefficients of the first and second layers, respectively, μ_{a1} and μ_{a2} indicate the absorption coefficients of the first and second layers, respectively, and $\Delta\mu_{a1}$ and $\Delta\mu_{a2}$ indicate the variations in the absorption coefficients in the first and second layers, respectively.

In the MC code, the photons were 'injected' in the two-layered slab and their trajectories traced according to statistical rules (Zaccanti 1991) until they were either detected or 'lost' (that is, they exited the medium without being detected). The photon was also considered 'lost' when the pathlength travelled in the medium was larger than a fixed value relevant for the geometry and optical properties chosen. Due to the symmetry of the medium, the detectors were chosen as rings of different radii centred at the source location. In most simulations the distances between the photon-injection point and the detectors were 1.0, 1.5, 2.0, 2.5 and 3 cm, which are values representative of typical source–detector distances employed in

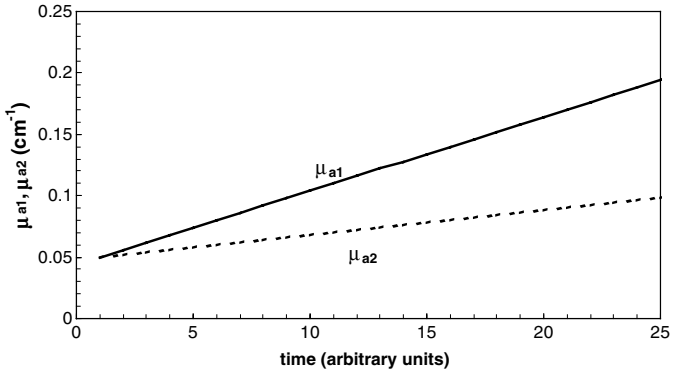

Figure 1. Example of temporal evolution of the absorption coefficients of the first (μ_{a1}) and second (μ_{a2}) layers for a MC simulation characterized by $\mu'_{s1} = 7\ \text{cm}^{-1}$, $\mu'_{s2} = 12\ \text{cm}^{-1}$ and thickness of the first layer $s_1 = 0.8$ cm.

measurements on tissue *in vivo*. For the simulation corresponding to the maximum thickness s_1 of 1.4 cm, we have added source–detector distances of 4.0 and 5.0 cm. For each detected photon we calculated the following complex weight W_j according to its time of flight (t_{fj}) and to the modulation frequency (f), which was set to 110 MHz in all the simulations presented in this work:

$$W_j = \exp(-\mu_{a1} l_{1j} - \mu_{a2} l_{2j}) \exp(i\omega t_{fj}) \tag{1}$$

where $\omega = 2\pi f$ is the angular modulation frequency, and $l_{1j}(l_{2j})$ is the pathlength spent in the first (second) layer. The time of flight is related to the total path length $l_{1j} + l_{2j}$ by the equation $t_{fj} = (l_{1j} + l_{2j})/v$, where v is the speed of the light in the medium, set in our simulations to 0.214 mm ps^{-1} (corresponding to a refractive index $n = 1.4$). In equation (1) j is a counter for the number of detected photons and i is the imaginary unit. After a given number of photons n_d were detected, the program stopped and the following total complex weight was calculated:

$$W = \frac{\sum_{j=1}^{n_d} W_j}{\Delta s N_t} \tag{2}$$

where Δs is the area of the ring detector and N_t is the total number of injected photons. The relevant parameters in the frequency domain, namely the ac and phase, are the amplitude and phase of W respectively, while the dc is the particular case of ac for $f = 0$.

The MC code was run for a non-absorbing case and the effect of the absorption coefficients was taken into account afterwards according to equation (1). In this way, it was straightforward to obtain the ac, dc and phase for different combinations of the absorption properties of the layers. The computation time required to calculate 50 different sets of ac, dc and phase corresponding to 50 different combinations of the absorption coefficients μ_{a1} and μ_{a2} was about 25 s for $n_d = 60\,000$ on a Pentium III (1 GHz, 1.5 GB RAM) personal computer.

For a better understanding of the calculations performed by the MC code, figure 1 shows an example of absorption traces $\mu_{a1}(t)$, $\mu_{a2}(t)$ (the time 't' is not an essential parameter of the simulations and it is introduced here only for convenience) used to calculate the ac, dc and phase temporal traces shown in figure 2 for a source–detector distance of 3 cm. The MC simulation of figures 1 and 2 was run for a medium with $s_1 = 0.8$ cm, $\mu'_{s1} = 7\ \text{cm}^{-1}$ and $\mu'_{s2} = 12\ \text{cm}^{-1}$. Our MC code also determines the average partial pathlengths $\langle L_1 \rangle$ and $\langle L_2 \rangle$ travelled by the photons in the first and second layers, respectively, which are important for some aspects of this work.

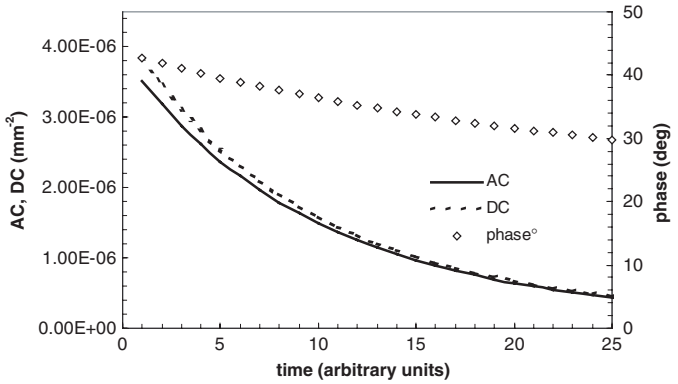

Figure 2. Traces of dc, ac and phase associated with the absorption changes of figure 1.

2.2. Data analysis

The ac, dc and phase data obtained with the Monte Carlo code have been used to calculate absorption variations according to three different models:

(a) a multidistance, frequency-domain method based on the diffusion theory (Fantini *et al* 1994) (in this work, we refer to this data analysis as 'multidistance method');
(b) a dpf, dc method based on a modified Lambert–Beer law (Matcher *et al* 1993) (in this work, we refer to this data analysis as 'dpf method');
(c) a two-distance, partial-pathlength extension of the dpf method for two-layered media (Hiraoka *et al* 1993) (in this work, we refer to this data analysis as 'dpf 2-ℓ method').

(a) The multidistance method is based on analytical expressions for the dependence of the ac, dc and phase on the optical properties of the medium (μ_a and μ_s') and the source–detector separation (r) (Fantini *et al* 1994). These expressions lead to the definition of three functions of the ac, dc and phase, respectively, that show a linear dependence on r. The optical coefficients μ_a and μ_s' can be expressed in terms of the slopes of such linear functions, S_{ac}, S_{dc} and S_ϕ, respectively. In particular, the absorption coefficient is given by the following equation (Fantini *et al* 1999):

$$\mu_a^{\text{eff}} = \frac{2\pi f}{2v}\left(\frac{S_\Phi}{S_{ac}} - \frac{S_{ac}}{S_\Phi}\right) \tag{3}$$

where f is the modulation frequency, v is the speed of light in the medium and the superscript 'eff' indicates an effective absorption coefficient in the case of inhomogeneous media. In this work, we have used the multidistance method to determine changes in the effective absorption coefficient $\left(\Delta\mu_a^{\text{eff}}\right)$ caused by variations of absorption in the two layers. Unless otherwise specified, we have applied equation (3) using ac and phase slopes obtained from a linear regression of the data at source–detector distances of 1.0, 1.5, 2.0 and 2.5 cm.

(b) The modified Lambert–Beer law allows for the calculation of the temporal changes in the absorption coefficient of a medium from the associated variations in the dc intensity (Matcher *et al* 1993); the modified Lambert–Beer law introduces the dpf, which is defined as the ratio between the photon mean pathlength ($\langle L\rangle$) in the medium and the geometrical distance between source and detector. The modified Lambert–Beer law assumes that the medium is homogeneous, the scattering changes are negligible and the absorption changes are small compared with the initial value of the absorption coefficient (Matcher *et al* 1993).

In this work, we have calculated the changes in the effective absorption coefficient obtained with the dpf method in two-layered media by using the following equation:

$$\Delta\mu_{\mathrm{a}}^{\mathrm{eff}}(t) = \Delta A(t)/\langle L\rangle \tag{4}$$

where $\Delta A(t)$ is the change in the optical density from time 0 to time t, defined as $\ln[\mathrm{dc}(0)/\mathrm{dc}(t)]$. In applying the dpf method, it is necessary to know the value of $\langle L\rangle$ in the medium. In our case, $\langle L\rangle$ is obtained from the Monte Carlo simulation for the initial optical properties of the medium, i.e. before introducing the variations in the absorption coefficients of the two layers. Variations in the absorption coefficient of a medium affect the value of $\langle L\rangle$, and in general one should take these variations of $\langle L\rangle$ into consideration. However, in the dpf method these variations are usually neglected and $\langle L\rangle$ is assumed to be a constant.

(c) The dpf method for a homogeneous medium can be extended to the case of a heterogeneous medium consisting of N regions individually homogeneous. In this heterogeneous case, the change in the optical density $\Delta A(t)$ can be written as follows (Hiraoka *et al* 1993):

$$\Delta A(t) = \sum\nolimits_{i=1}^{N} (\langle L_{\mathrm{i}}\rangle \Delta\mu_{\mathrm{ai}}(t)) \tag{5}$$

where $\langle L_{\mathrm{i}}\rangle$ is the partial pathlength in region i, and $\Delta\mu_{\mathrm{ai}}(t)$ is the variation of the absorption coefficient in region i between time 0 and time t. For a two-layered medium and considering two source–detector distances, equation (5) leads to the following two equations for each distance:

$$\begin{cases} \Delta A^{\mathrm{r1}}(t) = \left\langle L_1^{\mathrm{r1}}\right\rangle \Delta\mu_{\mathrm{a1}}(t) + \left\langle L_2^{\mathrm{r1}}\right\rangle \Delta\mu_{\mathrm{a2}}(t) \\ \Delta A^{\mathrm{r2}}(t) = \left\langle L_1^{\mathrm{r2}}\right\rangle \Delta\mu_{\mathrm{a1}}(t) + \left\langle L_2^{\mathrm{r2}}\right\rangle \Delta\mu_{\mathrm{a2}}(t) \end{cases} \tag{6}$$

where the subscripts '1' and '2' refer to the first and second layers, respectively, and the superscripts r1 and r2 indicate the two source–detector distances. By measuring changes in optical density at two different source–detector distances, one can use equation (6) to calculate the variations of the absorption coefficient in the two layers, provided that the partial pathlengths are known. In the data analysis based on the dpf 2-ℓ method, we have used the values of the partial pathlengths provided by the Monte Carlo simulation for the initial optical properties of the medium, before introducing variations in the absorption coefficients of the two layers. As in the standard dpf case, we have neglected the changes in the partial pathlengths and assumed constant values for $\langle L_{\mathrm{i}}\rangle$.

The dpf 2-ℓ method requires knowledge of the partial pathlengths in the two layers for the two source–detector distances, and this information is usually not available. However, for some applications it may still be possible to apply the dpf 2-ℓ method without necessarily having to assume the values of the partial pathlengths *a priori*. For example, if during a given time interval the absorption variations occur only in the first layer, then in this time interval equation (6) becomes:

$$\begin{cases} \Delta A^{\mathrm{r1}}(t) = \left\langle L_1^{\mathrm{r1}}\right\rangle \Delta\mu_{\mathrm{a1}}(t) \\ \Delta A^{\mathrm{r2}}(t) = \left\langle L_1^{\mathrm{r2}}\right\rangle \Delta\mu_{\mathrm{a1}}(t). \end{cases} \tag{7}$$

By taking the ratio of the two equations in equation (7), one can define a constant $K_1 = \left\langle L_1^{\mathrm{r2}}\right\rangle / \left\langle L_1^{\mathrm{r1}}\right\rangle$ which is experimentally accessible being given by the ratio $\Delta A^{\mathrm{r2}}(t)/\Delta A^{\mathrm{r1}}(t)$. When the absorption changes also in the second layer, the solution to equation (6) yields the following expression for $\Delta\mu_{\mathrm{a2}}$ in terms of K_1:

$$\Delta\mu_{\mathrm{a2}}(t) = \frac{\Delta A^{\mathrm{r2}}(t) - K_1 \Delta A^{\mathrm{r1}}(t)}{\left\langle L_2^{\mathrm{r2}}\right\rangle - K_1 \left\langle L_2^{\mathrm{r1}}\right\rangle}. \tag{8}$$

In the denominator of equation (8), there is a linear combination of the partial pathlengths in the second layer for the two source–detector distances. Because the partial pathlengths are assumed to be constant, $\Delta\mu_{a2}$ can be obtained to within a multiplicative factor (K_2) as follows:

$$\Delta\mu_{a2}(t) = K_2[\Delta A^{r2}(t) - K_1 \Delta A^{r1}(t)] \tag{9}$$

where $K_2 = \left(\left\langle L_2^{r2}\right\rangle - K_1\left\langle L_2^{r1}\right\rangle\right)^{-1}$. In near-infrared spectroscopy, there are cases, most notably the measurement of the oxygen saturation of haemoglobin, where it is relevant to be able to measure the absorption coefficient to within a multiplicative factor.

2.3. Cerebral near-infrared spectroscopy in vivo

We have recently reported the results of NIRS measurements of the concentration and oxygen saturation of haemoglobin on the right and left frontal brain regions of human subjects during right unilateral ECT (Fabbri *et al* 2003). The data were collected with a frequency-domain tissue spectrometer (OxiplexTS, ISS, Inc., Champaign, IL) using two optical probes placed on the forehead of the subject. We have collected data at four source–detector distances, namely 1.0, 1.5, 2.0 and 2.5 cm. A consistent result of this study was the cerebral deoxygenation on the side ipsilateral to the electrical ECT discharge (Fabbri *et al* 2003), which is applied for about 3 s to induce a generalized seizure. Such a deoxygenation is associated with a decrease in the absorption coefficient at 830 nm. A limitation of non-invasive NIRS measurements is that they are sensitive to absorption changes occurring in the brain as well as in superficial extracerebral layers (skin, scalp, skull, etc). As a result, it is sometimes difficult to discriminate the optical signals originating in the brain from those originating in more superficial tissue layers. With respect to the homogeneous case, a two-layered model is a step forward towards the goal of achieving depth discrimination. A comparison of the results of the methods of data analysis described in section 2.2 may help separate the cerebral haemodynamic response from contributions of superficial tissue layers. Here, we consider the data for one representative subject (a 39 year old male) analysed with all three methods (a), (b) and (c) described above.

3. Results

3.1. Results of the Monte Carlo simulations

Figures 3–6 compare the following absorption changes:

- the actual values of $\Delta\mu_{a1}$ and $\Delta\mu_{a2}$ (black continuous lines);
- the values of $\Delta\mu_a^{eff}$ (multidistance) calculated from ac and phase data at source–detector distances of 1.0–2.5 cm (open triangles in figures 3–5), 2.5–3.0 cm (filled triangles in figure 5) and 4.0–5.0 cm (open triangles in figure 6);
- the values of $\Delta\mu_a^{eff}$ (dpf) for a source–detector distance of 1.0 cm (filled circles in figures 3–6), 2.5 cm (filled squares in figures 3–5) and 5.0 cm (filled squares in figure 6);
- the values of $\Delta\mu_{a1}$ (dpf 2-ℓ) and $\Delta\mu_{a2}$ (dpf 2-ℓ) (open diamonds and open circles, respectively) calculated from data at source–detector distances of 1.0 and 2.5 cm (in figures 3–5), or 1.0 and 5.0 cm (in figure 6).

Panel (a) in figures 3–6 shows the thickness of the first layer, the source–detector distances and the initial optical coefficients of the two layers. The x-axis of panel (b) in figures 3–6 reports $\Delta\mu_{a2}/\mu_{a2}$, i.e. the relative variation in the absorption coefficient of the second layer. For every case presented in figures 3–6, we have calculated the percent relative difference between the actual absorption changes in the two layers and the absorption changes obtained by applying the multidistance, the dpf and the dpf 2-ℓ methods; these relative differences are

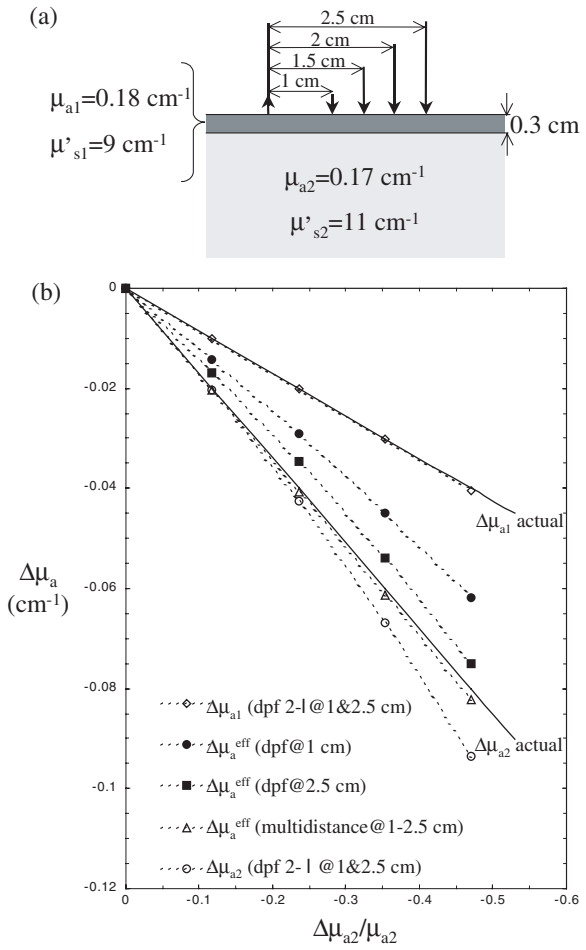

Figure 3. (a) Schematic illustration of the geometrical conditions and optical coefficients for the Monte Carlo simulation. (b) Comparison between the actual optical changes in the two layers ($\Delta\mu_{a1}$ and $\Delta\mu_{a2}$) and the absorption changes obtained from the simulated data using the multidistance, dpf and dpf 2-ℓ methods (see the text for the definition of all the symbols).

shown in tables 1–4, which correspond to the results of figures 3–6, respectively. Tables 1–4 consist of two parts. The first part refers to the second, underlying layer. The first column shows the actual $\Delta\mu_{a2}/\mu_{a2}$ and the other columns report the per cent differences between the actual values of $\Delta\mu_{a2}$ and the values of $\Delta\mu_{a2}$ $\left(\Delta\mu_a^{\text{eff}}\right)$ obtained with the dpf 2-ℓ method (multidistance or dpf method). The second part refers to the first, superficial layer. The first column shows the actual $\Delta\mu_{a1}/\mu_{a1}$ and the other columns show the per cent differences between the actual values of $\Delta\mu_{a1}$ and the values of $\Delta\mu_{a1}$ $\left(\Delta\mu_a^{\text{eff}}\right)$ obtained with the dpf 2-ℓ method (dpf method at a source–detector distance of 1 cm).

The results of figures 3–6 and tables 1–4 can be summarized as follows.

First-layer thickness of 0.3 cm. In the case of a 0.3 cm thick first layer (figure 3 and table 1), $\Delta\mu_a^{\text{eff}}$ obtained using the multidistance method is an excellent estimate of the actual $\Delta\mu_{a2}$, even considering strong variations in μ_{a2} (in table 1, the relative difference between $\Delta\mu_a^{\text{eff}}$

Table 1. Comparison between the actual optical changes in the two layers ($\Delta\mu_{a1}$ and $\Delta\mu_{a2}$) and the absorption changes obtained from Monte Carlo data using the multidistance, dpf and dpf 2-ℓ methods using the source–detector distances indicated. This table refers to the simulation case of figure 3.

$\Delta\mu_{a2}/\mu_{a2}$ actual (%)	$\delta\Delta\mu_{a2}/\Delta_{a2}$ dpf 2-ℓ @ 1 and 2.5 cm (%)	$\delta\Delta\mu_a^{eff}/\Delta\mu_{a2}$ multidistance @ 1–2.5 cm (%)	$\delta\Delta\mu_a^{eff}/\Delta\mu_{a2}$ dpf @ 2.5 cm (%)	$\Delta\mu_{a1}/\mu_{a1}$ actual (%)	$\delta\Delta\mu_{a1}/\Delta\mu_{a1}$ dpf 2-ℓ @ 1 and 2.5 cm (%)	$\delta\Delta\mu_a^{eff}/\Delta\mu_{a1}$ dpf @ 1 cm (%)
0	0	0	0	0	0	0
−11.8	2.3	1.5	−16.0	−5.6	0.1	42.0
−23.5	6.6	1.9	−13.2	−11.1	0.5	45.7
−35.3	11.5	2.3	−10.0	−16.7	0.9	49.8
−47.1	17.1	2.7	−6.3	−22.2	1.1	54.4

Table 2. Comparison between the actual optical changes in the two layers ($\Delta\mu_{a1}$ and $\Delta\mu_{a2}$) and the absorption changes obtained from Monte Carlo data using the multidistance, dpf and dpf 2-ℓ methods using the source–detector distances indicated. This table refers to the simulation case of figure 4.

$\Delta\mu_{a2}/\mu_{a2}$ actual (%)	$\delta\Delta\mu_{a2}/\Delta_{a2}$ dpf 2-ℓ @ 1 and 2.5 cm (%)	$\delta\Delta\mu_a^{eff}/\Delta\mu_{a2}$ multidistance @ 1–2.5 cm (%)	$\delta\Delta\mu_a^{eff}/\Delta\mu_{a2}$ dpf @ 2.5 cm (%)	$\Delta\mu_{a1}/\mu_{a1}$ actual (%)	$\delta\Delta\mu_{a1}/\Delta\mu_{a1}$ dpf 2-ℓ @ 1 and 2.5 cm (%)	$\delta\Delta\mu_a^{eff}/\Delta\mu_{a1}$ dpf @ 1 cm (%)
0	0	0	0	0	0	0
−8.0	−1.5	2.8	−43.6	−2.0	−4.1	53.9
−16.0	1.0	3.6	−42.4	−4.0	−3.6	56.1
−24.0	3.8	4.4	−41.2	−6.0	−3.5	58.5
−32.0	6.8	5.2	−39.8	−8.0	−3.3	61.0

Table 3. Comparison between the actual optical changes in the two layers ($\Delta\mu_{a1}$ and $\Delta\mu_{a2}$) and the absorption changes obtained from Monte Carlo data using the multidistance, dpf and dpf 2-ℓ methods using the source–detector distances indicated. This table refers to the simulation case of figure 5.

$\Delta\mu_{a2}/\mu_{a2}$ actual (%)	$\delta\Delta\mu_{a2}/\Delta_{a2}$ dpf 2-ℓ @ 1 and 2.5 cm (%)	$\delta\Delta\mu_a^{eff}/\Delta\mu_{a2}$ multidistance @ 1–2.5 cm (%)	$\delta\Delta\mu_a^{eff}/\Delta\mu_{a2}$ multidistance @ 2.5–3 cm (%)	$\Delta\mu_a^{eff}/\mu_{a2}$ dpf @ 2.5 cm (%)	$\Delta\mu_{a1}/\mu_{a1}$ actual (%)	$\delta\Delta\mu_{a1}/\Delta\mu_{a1}$ dpf 2-ℓ @ 1 and 2.5 cm (%)	$\delta\Delta\mu_a^{eff}/\Delta\mu_{a1}$ dpf @ 1 cm (%)
0	0	0	0	0	0	0	0
−8.0	−2.8	−33.9	−16.9	−54.8	−2.0	−2.2	26.8
−16.0	0.4	−32.9	−16.0	−53.9	−4.0	−2.1	28.2
−24.0	3.7	−31.8	−15.2	−52.9	−6.0	−1.9	29.7
−32.0	7.4	−30.7	−14.3	−51.9	−8.0	−1.8	31.3

and the actual $\Delta\mu_{a2}$ is 2.7% for a relative variation of −47.1% in μ_{a2}). For the conditions of our simulation, the values of $\Delta\mu_{a2}$ obtained using the dpf 2-ℓ method are good estimates of the actual values of $\Delta\mu_{a2}$ only if the relative decrease in μ_{a2} is <25%. In fact, the relative difference between $\Delta\mu_{a2}$ (dpf 2-ℓ) and the actual $\Delta\mu_{a2}$ is 6.6% for a relative variation of −23.5% in μ_{a2}, but the relative difference becomes as high as 17.1% for a relative variation of −47.1% in μ_{a2}. The values of $\Delta\mu_a^{eff}$ obtained using the dpf method deviate significantly from the actual $\Delta\mu_{a2}$ even considering little variations in μ_{a2} (the relative difference between $\Delta\mu_a^{eff}$ and the actual $\Delta\mu_{a2}$ is −16% for a relative variation of −11.8% in μ_{a2}).

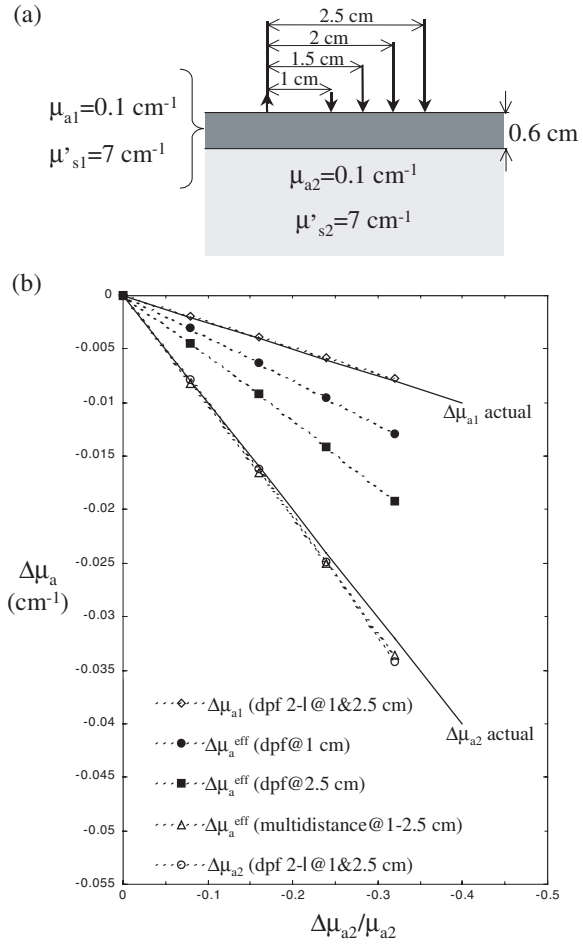

Figure 4. (a) Schematic illustration of the geometrical conditions and optical coefficients for the Monte Carlo simulation. (b) Comparison between the actual optical changes in the two layers ($\Delta\mu_{a1}$ and $\Delta\mu_{a2}$) and the absorption changes obtained from the simulated data using the multidistance, dpf and dpf 2-ℓ methods (see the text for the definition of all the symbols).

Table 4. Comparison between the actual optical changes in the two layers ($\Delta\mu_{a1}$ and $\Delta\mu_{a2}$) and the absorption changes obtained from Monte Carlo data using the multidistance, dpf and dpf 2-ℓ methods using the source–detector distances indicated. This table refers to the simulation case of figure 6.

$\Delta\mu_{a2}/\mu_{a2}$ actual (%)	$\delta\Delta\mu_{a2}/\Delta_{a2}$ dpf 2-ℓ @ 1 and 5 cm (%)	$\delta\Delta\mu_a^{eff}/\Delta\mu_{a2}$ multidistance @ 4–5 cm (%)	$\delta\Delta\mu_a^{eff}/\Delta\mu_{a2}$ dpf @ 5 cm (%)	$\Delta\mu_{a1}/\mu_{a1}$ actual (%)	$\delta\Delta\mu_{a1}/\Delta\mu_{a1}$ dpf 2-ℓ @ 1 and 5 cm (%)	$\delta\Delta\mu_a^{eff}/\Delta\mu_{a1}$ dpf @ 1 cm (%)
0	0	0	0	0	0	0
−11.1	3.8	−48.3	−44.9	−7.1	0.1	0.5
−22.2	13.6	−38.3	−43.5	−14.3	1.4	1.7
−33.3	25.4	−33.6	−41.8	−21.4	2.6	3.1
−44.4	39.6	−30.2	−39.8	−28.6	4.0	4.5

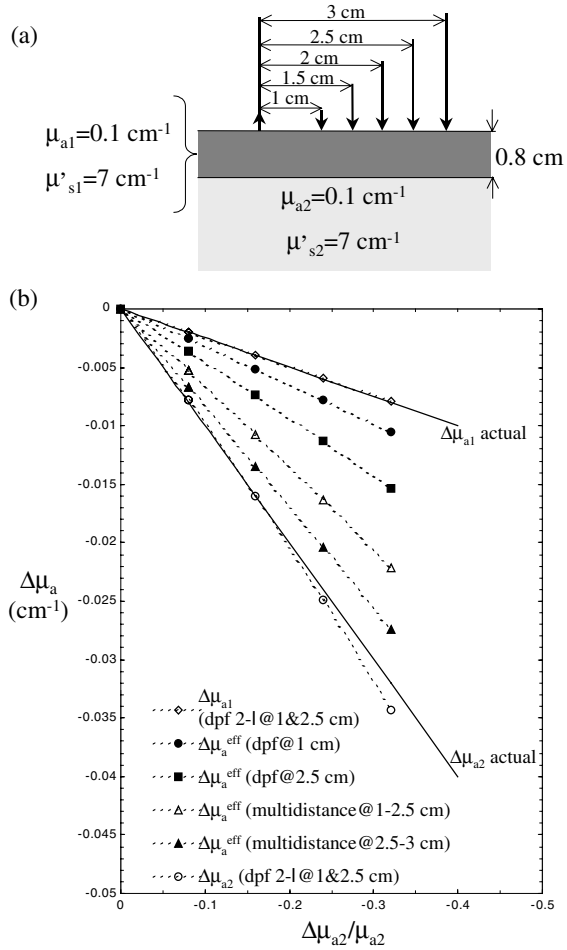

Figure 5. (a) Schematic illustration of the geometrical conditions and optical coefficients for the Monte Carlo simulation. (b) Comparison between the actual optical changes in the two layers ($\Delta\mu_{a1}$ and $\Delta\mu_{a2}$) and the absorption changes obtained from the simulated data using the multidistance, dpf and dpf 2-ℓ methods (see the text for the definition of all the symbols).

First-layer thickness of 0.6 cm. Figure 4 and table 2 refer to a two-layered medium with a first layer that is 0.6 cm thick. In this case, the values of $\Delta\mu_a^{\text{eff}}$ and $\Delta\mu_{a2}$ obtained using the multidistance and the dpf 2-ℓ methods, respectively, are good estimates of the actual $\Delta\mu_{a2}$, even for large variations in μ_{a2}. In fact, the relative difference between the multidistance $\Delta\mu_a^{\text{eff}}$ ($\Delta\mu_{a2}$-dpf 2-ℓ) and the actual $\Delta\mu_{a2}$ is 5.2% (6.8%) for a relative variation of -32% in μ_{a2}. The values of $\Delta\mu_a^{\text{eff}}$ obtained using the dpf method are significantly different than the actual $\Delta\mu_{a2}$ (the relative difference between $\Delta\mu_a^{\text{eff}}$ and the actual $\Delta\mu_{a2}$ is -43.6% for a relative variation of -8% in μ_{a2}).

First-layer thickness of 0.8 cm. Figure 5 and table 3 refer to a two-layered medium with a first layer that is 0.8 cm thick. In this case, $\Delta\mu_{a2}$ obtained using the dpf 2-ℓ methods is a good estimate of the actual $\Delta\mu_{a2}$ (the relative difference between $\Delta\mu_{a2}$ (dpf 2-ℓ) and the actual $\Delta\mu_{a2}$ is 7.4% for a relative variation of -32% in μ_{a2}). The values of $\Delta\mu_a^{\text{eff}}$ calculated using the multidistance method over distances of 1.0–2.5 cm deviate significantly from the

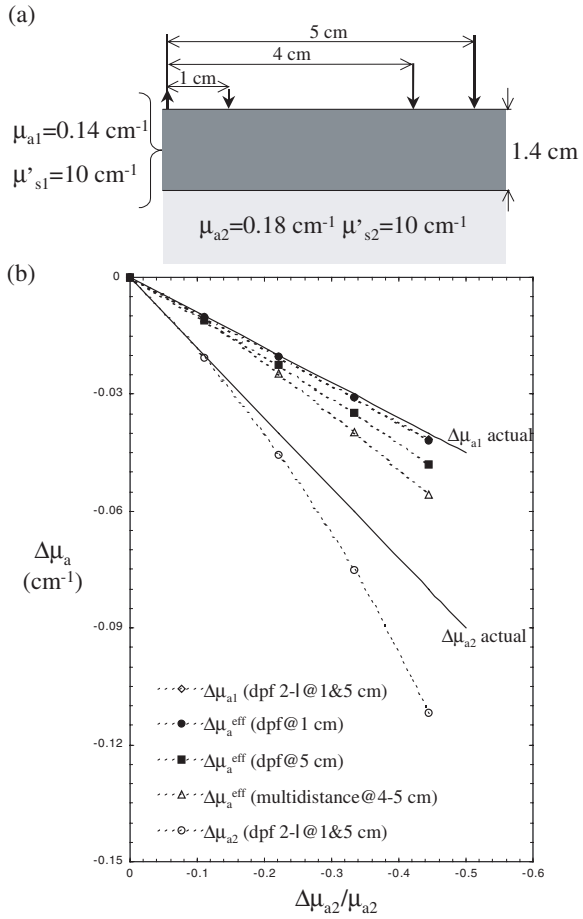

Figure 6. (a) Schematic illustration of the geometrical conditions and optical coefficients for the Monte Carlo simulation. (b) Comparison between the actual optical changes in the two layers ($\Delta\mu_{a1}$ and $\Delta\mu_{a2}$) and the absorption changes obtained from the simulated data using the multidistance, dpf and dpf 2-ℓ methods (see the text for the definition of all the symbols). In the graph, open diamonds and filled circles are superimposed.

actual $\Delta\mu_{a2}$ (the relative difference between $\Delta\mu_a^{\text{eff}}$ and the actual $\Delta\mu_{a2}$ is -33.9% for a relative variation of -8% in μ_{a2}); a better agreement between the actual $\Delta\mu_{a2}$ and $\Delta\mu_a^{\text{eff}}$ can be found if $\Delta\mu_a^{\text{eff}}$ is calculated using data collected at source–detector distances of 2.5 and 3.0 cm (in this case, the relative difference between $\Delta\mu_a^{\text{eff}}$ and the actual $\Delta\mu_{a2}$ is -16.9% for a relative variation of -8% in μ_{a2}). This fact indicates that for a first-layer thickness of 0.8 cm, the absorption measurements performed with the multidistance method at source–detector distances shorter than 2.5 cm are affected by absorption variations that occur in the first layer. Finally, $\Delta\mu_a^{\text{eff}}$ obtained with the dpf method presents large differences with the actual $\Delta\mu_{a2}$ (55% for a relative variation of -8% in μ_{a2}).

First-layer thickness of 1.4 cm. Figure 6 and table 4 refer to the case of a two-layered medium with a first layer that is 1.4 cm thick. In this case, $\Delta\mu_a^{\text{eff}}$ obtained using the multidistance

and the dpf methods is strongly affected by absorption variations that occur in the first layer even using data at source–detector distances as high as 4.0–5.0 cm. For a relative variation of -11.1% in μ_{a2} the relative difference between $\Delta\mu_a^{eff}$ (obtained using the multidistance method at distances of 4.0 and 5.0 cm) and the actual $\Delta\mu_{a2}$ is -48.3%, and the relative difference between $\Delta\mu_a^{eff}$ (obtained using the dpf method at a distance of 5 cm) and the actual $\Delta\mu_{a2}$ is -44.9%. For the conditions of our simulations, the values of $\Delta\mu_{a2}$ obtained using the dpf 2-ℓ method are good estimates of the actual values of $\Delta\mu_{a2}$ only if the actual relative decrease in μ_{a2} is $<20\%$. In fact, the relative difference between $\Delta\mu_{a2}$ (dpf 2-ℓ) and the actual $\Delta\mu_{a2}$ is 13.6% for a relative variation of -22.2% in μ_{a2}, but the relative difference is as high as 39.6% for a relative variation of -44% in μ_{a2}.

In all the cases presented here, $\Delta\mu_a^{eff}$ obtained using the dpf method at a source–detector distance of 2.5 cm presents relative deviations from the actual $\Delta\mu_{a2}$ that are larger (in absolute value) than those of the multidistance method. This fact indicates that the dpf method is affected more than the multidistance method by variations that occur in a superficial layer. Figures 3–6 show that in all the cases considered here, the data obtained using the dpf and the dpf 2-ℓ methods deviate appreciably from linearity when the relative changes in μ_{a2} are approximately greater than 20–30%. The reason for this deviation from linearity is that we have considered constant values of the partial pathlengths in the medium. In fact, as we have already noted, the dpf method requires that the variations in μ_{a2} be small. We point out that the assumption of constant partial pathlengths is the only source of error for the dpf 2-ℓ method applied to the simulated data. Furthermore, in all the cases presented here, we have found that the values of $\Delta\mu_{a1}$ obtained using the dpf 2-ℓ method are in excellent agreement (to within a few per cent) with the actual values of $\Delta\mu_{a1}$. By contrast, $\Delta\mu_a^{eff}$ obtained using the dpf method at a source–detector distance of 1 cm is in good agreement with the actual values of $\Delta\mu_{a1}$ only for the largest first-layer thickness of 1.4 cm.

The dpf 2-ℓ method of data analysis requires the values of the partial pathlengths in the two layers for each source–detector distance. In our simulations, these partial pathlengths have been provided by the Monte Carlo simulations on the basis of the thickness s_1 of the first layer and the initial optical properties of the medium (μ_{a1}, μ_{a2}, μ'_{s1}, μ'_{s2}). If the initial optical properties of the medium are not known exactly, the errors in these values will affect the partial pathlengths and, in turn, the values of $\Delta\mu_{a1}$ and $\Delta\mu_{a2}$ calculated using the dpf 2-ℓ method. To obtain quantitative indications on the sensitivity of $\Delta\mu_{a1}$ and $\Delta\mu_{a2}$ obtained with the dpf 2-ℓ method to the initial values of the optical coefficients, we have considered one more Monte Carlo simulation. In this simulation, $s_1 = 0.8$ cm, $\mu_{a1} = 0.05$ cm^{-1}, $\mu_{a2} = 0.05$ cm^{-1}, $\mu'_{s1} = 5.5$ cm^{-1}, $\mu'_{s2} = 5.5$ cm^{-1}, and the source-detector distances are 1.0 and 2.5 cm. Table 5 reports the per cent variations in the partial pathlengths caused by varying, one at a time, μ_{a1}, μ_{a2}, μ'_{s1}, and μ'_{s2} to within $\pm 20\%$. In table 5, like in equation (6), the partial pathlengths are identified with $\langle L_1^{r1}\rangle$, $\langle L_2^{r2}\rangle$, $\langle L_1^{r2}\rangle$, and $\langle L_2^{r2}\rangle$, where the subscripts 1 and 2 indicate the first and the second layer, respectively, whereas the superscripts r1 and r2 indicate the source–detector distances of 1.0 and 2.5 cm, respectively. In table 5, all the variations are identified with the symbol δ. In the last row of table 5, one can see that inaccuracies within $\pm 20\%$ in the initial values of the optical properties cause maximum per cent error in the partial pathlengths of 5.8%, 12.4%, 8.4% and 13.9% for $\langle L_1^{r1}\rangle$, $\langle L_2^{r1}\rangle$, $\langle L_1^{r2}\rangle$, and $\langle L_2^{r2}\rangle$, respectively (in this calculation we have taken the absolute values of the variations). Errors in the partial pathlengths propagate into errors in the optical coefficients yielded by the dpf 2-ℓ method. Figure 7 compares the values of $\Delta\mu_{a1}$ and $\Delta\mu_{a2}$ obtained using the dpf 2-ℓ method with the actual values of $\Delta\mu_{a1}$ and $\Delta\mu_{a2}$ for the cases of a relative error of -20% in either μ_{a2} or μ'_{s1}.

Table 5. Relative deviations in the partial pathlengths in the two layers ($\langle L_1^{r1}\rangle$, $\langle L_2^{r1}\rangle$, $\langle L_1^{r2}\rangle$, $\langle L_2^{r2}\rangle$) associated with errors in the assumed initial optical properties of the two layers (μ_{a1}, μ_{a2}, μ'_{s1} and μ'_{s2}). This table refers to the simulation case of figure 7. The subscripts in the partial pathlengths specify the layer, while the superscripts indicate the source–detector distance ($r1 = 1$ cm, $r2 = 2.5$ cm). The last row shows the absolute value of the maximum deviation in the partial pathlengths.

$\delta\mu_{a1}/\mu_{a1}$ (%)	$\delta\mu_{a2}/\mu_{a2}$ (%)	$\delta\mu'_{s1}/\mu'_{s1}$ (%)	$\delta\mu'_{s2}/\mu'_{s2}$ (%)	$\delta\langle L_1^{r1}\rangle/\langle L_1^{r1}\rangle$ (%)	$\delta\langle L_2^{r1}\rangle/\langle L_2^{r1}\rangle$ (%)	$\delta\langle L_1^{r2}\rangle/\langle L_1^{r2}\rangle$ (%)	$\delta\langle L_2^{r2}\rangle/\langle L_2^{r2}\rangle$ (%)
−20	–	–	–	2.2	4.1	2.2	0.8
−10	–	–	–	1.1	2.0	1.1	0.4
10	–	–	–	−1.0	−1.9	−1.1	−0.3
20	–	–	–	−2.0	−3.8	−2.1	−0.7
–	−20	–	–	0.9	12.4	0.5	13.9
–	−10	–	–	0.4	5.8	0.2	6.5
–	10	–	–	−0.4	−5.2	−0.2	−5.8
–	20	–	–	−0.8	−9.8	−0.4	−11.0
–	–	−18	–	−5.8	11.0	−8.4	−8.8
–	–	−9	–	−3.2	4.4	−4.3	−3.9
–	–	9	–	2.8	−1.5	3.4	3.7
–	–	18	–	5.7	−5.8	7.4	8.8
–	–	–	−18	−2.2	−5.1	−3.8	0.6
–	–	–	−9	−0.6	−2.5	−1.7	0.4
–	–	–	9	1.0	1.8	0.9	−1.4
–	–	–	18	2.3	5.5	2.1	−1.8
				Max	Max	Max	Max
				5.8	12.4	8.4	13.9

3.2. Representative results in vivo

The results obtained from near-infrared data collected *in vivo* on the forehead of a human subject during ECT are shown in figure 8. Figure 8(a) shows a comparison between $\Delta\mu_a^{eff}$ (at 830 nm) obtained with the multidistance, frequency-domain method and $\Delta\mu_a^{eff}$ obtained with the dpf method from dc data at a source–detector distance of 2.5 cm. The values of $\Delta\mu_a^{eff}$ are set to the same peak value at time 140 s, which is just before the delivery of the electrical discharge (indicated by a dashed line in figure 8), by introducing a multiplicative normalization factor. Although the two curves in figure 8(a) are similar, one can observe some qualitative differences. In particular, we focus our attention on the temporal traces following the ECT electrical discharge, when the electrically induced seizure is definitely causing absorption changes in the brain tissue (which in our two-layer model corresponds to the bottom layer). After the ECT electrical discharge, $\Delta\mu_a^{eff}$(multidistance) shows a strong decrease followed by a recovery that fully compensates the initial decrease, so that $\Delta\mu_a^{eff}$(multidistance) at the end of the measurement (time ∼210–220 s) is back to the pre-discharge value. By contrast, the strong decrease that occurs in $\Delta\mu_a^{eff}$(dpf) after the electrical discharge is not compensated by the following increase, so that $\Delta\mu_a^{eff}$(dpf) does not fully recover to the predischarge value. The lower recovery value of $\Delta\mu_a^{eff}$(dpf) with respect to the predischarge value was also observed for $\Delta\mu_a^{eff}$(dpf) obtained at a source–detector distance of 1.0 cm (data not shown), which is mostly sensitive to extracerebral, superficial tissue. Because it has been shown that the multidistance method is relatively insensitive to absorption variations that occur in a superficial layer 0.4–0.6 cm thick (Franceschini *et al* 1998), it is reasonable to attribute the differences between the curves of $\Delta\mu_a^{eff}$ obtained with the dpf (at 2.5 cm) and the multidistance methods to absorption variations that occur in the most superficial tissue.

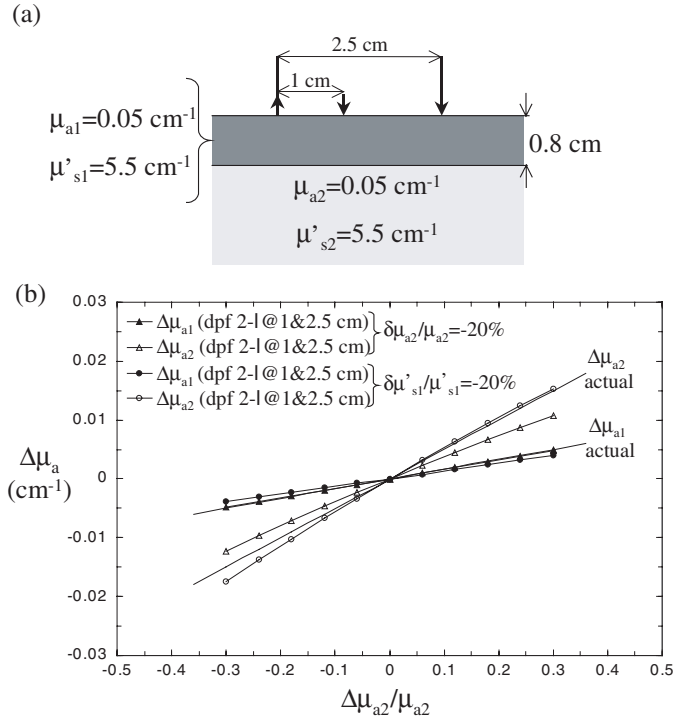

Figure 7. (a) Schematic illustration of the geometrical conditions and optical coefficients for the Monte Carlo simulation. (b) Comparison between the actual optical changes in the two layers ($\Delta\mu_{a1}$ and $\Delta\mu_{a2}$) and the corresponding values obtained with the dpf 2-ℓ method using initial estimates of μ_{a2} and μ'_{s1} that are off by -20% with respect to the actual values.

As an alternative approach to increase in the selective sensitivity to the underlying brain tissue as opposed to more superficial tissue, we have applied the modified Lambert–Beer law for a two-layered medium (equation (6)) using the data collected at source–detector distances of 1.0 and 2.5 cm. Because we did not know the partial pathlengths in the two layers with which we are modelling the tissue, we have followed the alternative approach described at the end of section 2.2. We have assumed that in the first 30 s of the measurement period, corresponding to baseline acquisition, the variations in the optical signals are mainly caused by absorption changes localized in superficial, extracerebral tissue. We have applied equation (7) to the data acquired in the first 30 s and we have calculated K_1 by taking an average of the ratio $\Delta A^{r2}(t)/\Delta A^{r1}(t)$ over the time range 0–30 s; we have obtained $K_1 = 1.2 \pm 0.2$ (average $\pm$ standard deviation), and the relatively small standard deviation indicates that K_1 can be considered constant with a good approximation. We have then applied equation (9) to the data acquired after the first 30 s to determine $\Delta\mu_{a2}$ to within a multiplicative factor. Figure 8(b) shows a comparison between the temporal trace of $\Delta\mu_{a2}$ calculated with this dpf 2-ℓ approach and $\Delta\mu_a^{eff}$ obtained with the multidistance method. As in figure 8(a), the curves in figure 8(b) have been normalized to the same peak value at time 140 s. The two curves in figure 8(b) show a good, quantitative agreement with the only exception of a smaller post-ECT-discharge decrease in μ_{a2}(dpf 2-ℓ) than in $\mu_a{}^{eff}$(multidistance). In particular, both dpf 2-ℓ and multidistance methods yield an absorption trace that fully recovers to the predischarge value.

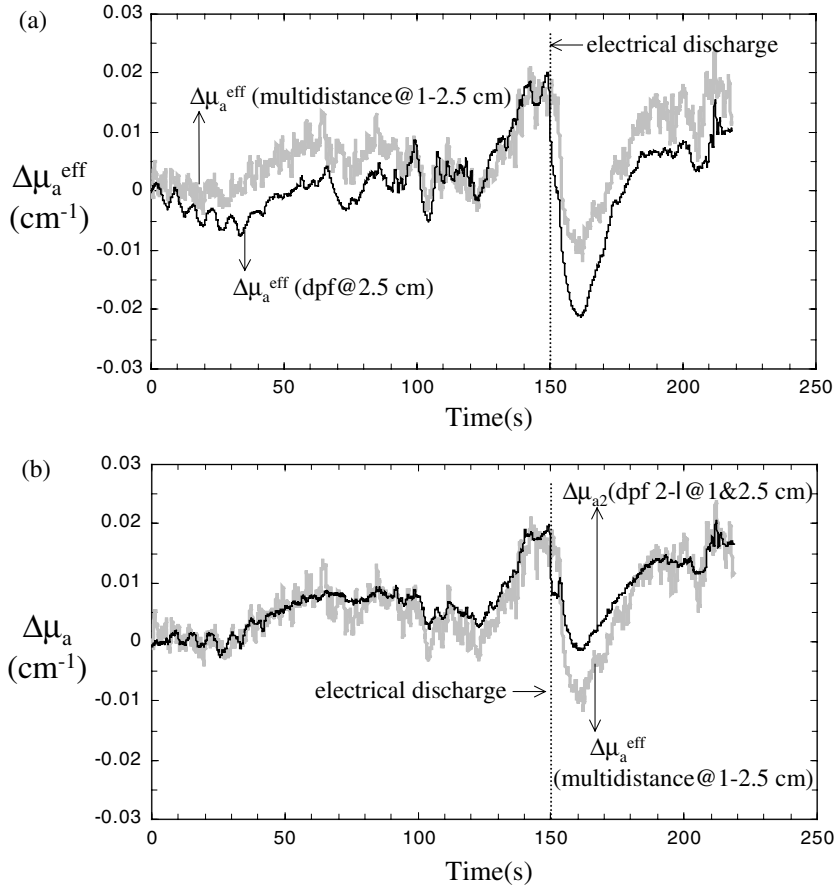

Figure 8. Results of the analysis of *in vivo* near-infrared data collected on the forehead of a human subject during ECT. The time of the ECT electrical discharge is indicated by the vertical dashed line. Comparison between the absorption changes obtained with the multidistance method and (a) the dpf method and (b) the dpf 2-ℓ method. The source–detector distances used in each method of data analysis are indicated in the figure.

4. Discussion

The results of the Monte Carlo simulations performed on a two-layered medium that are reported in figures 3–6 and tables 1–4 show that that the dpf method is more affected than the multidistance method by absorption variations that occur in the first layer, at least for source–detector distances in the range 1.0–2.5 cm, and first-layer thicknesses in the range 0.3–0.8 cm. As a result, the values of $\Delta\mu_a^{\rm eff}$ obtained with the dpf method are intermediate between the actual values of $\Delta\mu_{a1}$ and $\Delta\mu_{a2}$. In the case of the thickest superficial layer (1.4 cm), the value of $\Delta\mu_a^{\rm eff}$ obtained with the dpf method at a source–detector distance of 1.0 cm is representative of the first layer. The sensitivity of the dpf method to absorption variations in superficial tissues may confound a measurement of absorption changes in deeper tissue structures such as skeletal muscle or brain. By contrast, for first-layer thicknesses up to 0.6–0.8 cm, the multidistance method yields absorption changes that are representative of the underlying layer, in agreement with (Franceschini *et al* 1998). The dpf 2-ℓ method, which

yields absorption changes for both layers, provides excellent estimates for the actual $\Delta\mu_{a1}$ in all the cases considered. The values of $\Delta\mu_{a2}$ obtained with the dpf 2-ℓ method deviate by no more than 8% from the actual $\Delta\mu_{a2}$ for the intermediate first-layer thicknesses of 0.6 and 0.8 cm, whereas they are within 10% of the actual $\Delta\mu_{a2}$ for relative variations in $\Delta\mu_{a2}$ that are <20–30% for first-layer thicknesses of 0.3 and 1.4 cm. In particular, the dpf 2-ℓ method is more accurate than the multidistance method in measuring the absorption changes underneath a superficial layer 0.8 or 1.4 cm thick, whereas the multidistance method is more accurate for a thin layer of 0.3 cm. However, we stress that the dpf 2-ℓ method assumes that the scattering changes are negligible and that the partial pathlengths in the two layers are known for each source–detector distance. To estimate the partial pathlengths, one can use Monte Carlo simulations for a given thickness of the first layer and optical properties of both layers. The effects on the measured absorption changes of inaccurate guesses for the optical coefficients are reported in figure 7 and table 4, considering the case of a two-layered medium with optical properties representative of those of biological tissue and a first-layer thickness of 0.8 cm. Of course, actual measurements *in vivo* may be further complicated by the unknown thickness of the first layer, and by an irregular and/or strongly inhomogeneous structure.

In section 3.2, we have reported the results of the analysis of near-infrared data collected on the forehead of a human subject during electroconvulsive therapy according to the dpf and multidistance methods. These two methods have yielded traces of $\Delta\mu_a^{\text{eff}}$ (see figure 8(a)) that present qualitative differences (most notably, the different post-discharge recovery value). On the basis of the Monte Carlo results, these differences can be attributed, at least in part, to absorption variations in the superficial extracerebral tissue, which have stronger effects on the results of the dpf method of data analysis. The same near-infrared data have been used to illustrate the alternative implementation of the dpf 2-ℓ method based on equation (9), which does not require knowledge of the partial pathlengths in the two layers. It only requires the collection of data during a time interval in which the absorption of the first layer changes and the absorption of the second layer remains constant. In the data analysis reported in figure 8(b), we assume that such time interval is 0–30 s. Here, we do not introduce any physiological arguments to justify this choice, but we point out that it is consistent with the fact that during the time interval 0–30 s, $\Delta\mu_a^{\text{eff}}$(multidistance) and $\Delta\mu_{a2}$(dpf 2-ℓ) are relatively constant while $\Delta\mu_a^{\text{eff}}$(dpf) decreases significantly. The point of the analysis reported in figure 8(b) is to illustrate the application of this alternative implementation of the dpf 2-ℓ method to *in vivo* data. One may envision experimental protocols specifically designed to induce superficial absorption changes to apply this alternative method more convincingly. The application of the dpf 2-ℓ method can provide additional insight for the interpretation of optical data *in vivo*, in particular about the depth at which optical signals are originated inside the tissue. For example, figure 8(b) shows the excellent agreement between the traces of $\Delta\mu_{a2}$(dpf 2-ℓ) and $\Delta\mu_a^{\text{eff}}$(multidistance) over most of the recording period. This agreement further suggests that the qualitative differences observed in figure 8(a) between $\Delta\mu_a^{\text{eff}}$(multidistance) and $\Delta\mu_a^{\text{eff}}$(dpf) result from absorption variations in more superficial, extracerebral tissue. The main difference between $\Delta\mu_{a2}$(dpf 2-ℓ) and $\Delta\mu_a^{\text{eff}}$(multidistance) in figure 8(b) is the stronger post-discharge decrease of $\Delta\mu_a^{\text{eff}}$(multidistance) with respect to $\Delta\mu_{a2}$(dpf 2-ℓ). This difference may be the result of the different sensitivity of $\Delta\mu_{a2}$(dpf 2-ℓ) and $\Delta\mu_a^{\text{eff}}$(multidistance) to superficial absorption changes, especially if they occur on a relatively thick layer of 0.8–1.4 cm (see figures 5 and 6). However, there may also be errors in $\Delta\mu_{a2}$(dpf 2-ℓ) from the likely violation of the assumptions of constant scattering and small absorption changes during the massive neuronal activation associated with the electrically induced seizure.

5. Conclusion

We have reported a study based on Monte Carlo simulations to compare different optical methods for the measurement of absorption changes in two-layered diffusive media. These optical methods either provide a single, effective absorption change (dpf method, multidistance method) or two absorption changes associated with each layer (dpf 2-ℓ). We have found that if one is interested in measuring the absorption changes in the underlying layer, the multidistance and the dpf 2-ℓ methods are the most effective ones in minimizing or separating the contributions from the absorption changes in the superficial layer. While the dpf 2-ℓ method is able to separately measure the absorption changes in the two layers, it is based on assumptions (no scattering changes, knowledge of the partial optical pathlengths in the two layers) that may limit its applicability. By contrast, the multidistance method may in some cases be more affected by the absorption changes in the superficial layer, but is of more general applicability. The application of these methods of data analysis to near-infrared data collected *in vivo* illustrates the different information content of the data processed according to the different methods.

Acknowledgments

Francesco Fabbri and Angelo Sassaroli have contributed equally to this paper. We thank the nursing staff at McLean Hospital for their technical assistance during the ECT measurement, and Dr Maria Angela Franceschini for her contribution to the collection of the near-infrared data during ECT. We acknowledge support from the National Institutes of Health (grant no. DA14178) and from the National Science Foundation (award no. BES-93840).

References

Bluestone A Y, Abdoulaev G, Schmitz C H, Barbour R L and Hielscher A H 2001 Three-dimensional optical tomography of hemodynamics in the human head *Opt. Exp.* **9** 272–86

Delpy D T and Cope M 1997 Quantification in tissue near-infrared spectroscopy *Phil. Trans. R. Soc.* B **352** 649–59

Fabbri F, Henry M E, Renshaw P F, Nadgir S, Ehrenberg B L, Franceschini M A and Fantini S 2003 Bilateral near-infrared monitoring of the cerebral concentration and oxygen-saturation of hemoglobin during right unilateral electro-convulsive therapy *Brain Res.* **992** 193–204

Fantini S, Franceschini M A and Gratton E 1994 Semi-infinite-geometry boundary problem for light migration in highly scattering media: a frequency-domain study in the diffusion approximation *J. Opt. Soc. Am.* B **11** 2128–38

Fantini S, Hueber D, Franceschini M A, Gratton E, Rosenfeld W, Stubblefield P G, Maulik D and Stankovic M R 1999 Non-invasive optical monitoring of the newborn piglet brain using continuous-wave and frequency-domain spectroscopy *Phys. Med. Biol.* **44** 1543–63

Ferrari M, Binzoni T and Quaresima V 1997 Oxidative metabolism in muscle *Phil. Trans. R. Soc.* B **352** 677–83

Franceschini M A, Fantini S, Paunescu L A, Maier J S and Gratton E 1998 Influence of a superficial layer in the quantitative spectroscopic study of strongly scattering media *Appl. Opt.* **37** 7447–58

Gopinath S P, Robertson C S and Grossman R G 1993 Near-infrared spectroscopic localization of intracranial hematomas *J. Neurosurg.* **79** 43–7

Gratton E, Fantini S, Franceschini M A, Gratton G and Fabiani M 1997 Measurements of scattering and absorption changes in muscle and brain *Phil. Trans. R. Soc.* B **352** 727–35

Gratton G, Maier J S, Fabiani M, Mantulin W W and Gratton E 1994 Feasibility of intracranial near-infrared optical scanning *Psychophysiology* **31** 211–5

Handbook of Optical Biomedical Diagnostics 2002 ed V V Tuchin (Bellingham, WA: SPIE) ch 7, 8, 9

Haskell R C, Svaasand L O, Tsay T, Feng T, McAdams M S and Tromberg B J 1994 Boundary conditions for the diffusion equation in radiative transfer *J. Opt. Soc. Am.* A **11** 2727–42

Hillman E M C, Hebden J C, Schweiger M, Dehghani H, Schmidt F E W, Delpy D T and Arridge S 2001 Time resolved optical tomography of the human forearm *Phys. Med. Biol* **46** 1117–30

Hiraoka M, Firbank M, Essenpreis M, Cope M, Arridge S R, van der Zee P and Delpy D T 1993 A Monte Carlo investigation of optical pathlength in inhomogeneous tissue and its application to near-infrared spectroscopy *Phys. Med. Biol.* **38** 1859–76

Jöbsis F F 1977 Noninvasive, infrared monitoring of cerebral and myocardial oxygen sufficiency and circulatory parameters *Science* **198** 1264–7

Maki A, Yamashita Y, Ito Y, Watanabe E, Mayanagi Y and Koizumi H 1995 Spatial and temporal analysis of human motor activity using noninvasive NIR topography *Med. Phys.* **22** 1997–2005

Matcher S J, Cope M and Delpy D T 1993 Use of the water absorption spectrum to quantify tissue chromophores concentration changes in near-infrared spectroscopy *Phys. Med. Biol.* **38** 177–96

Meek J H, Elwell C E, Khan M J, Romaya J, Wyatt J S, Delpy D T and Zeki S 1995 Regional changes in cerebral haemodynamics as a result of a visual stimulus measured by near infrared spectroscopy *Proc. R. Soc.* B **261** 351–6

Obrig H, Wenzel R, Kohl M, Horst S, Wobst P, Steinbrink J, Thomas F and Villringer A 2000 Near-infrared spectroscopy: does it function in functional activation studies of the adult brain? *Int. J. Psychophysiol.* **35** 125–42

Okada E, Firbank M, Schweiger M, Arridge S R, Cope M and David T Delpy 1997 Theoretical and experimental investigation of near-infrared light propagation in a model of the adult head *Appl. Opt.* **36** 21–31

Patterson M S, Chance B and Wilson B C 1989 Time resolved reflectance and transmittance for the noninvasive measurement of tissue optical properties *Appl. Opt.* **28** 2331–6

Testorf M, Osterberg U, Pogue B and Paulsen K 1999 Sampling of time-and frequency-domain signals in Monte Carlo simulations of photon migration *Appl. Opt.* **38** 236–45

Villringer A and Chance B 1997 Non-invasive optical spectroscopy and imaging of human brain function *Trends Neurosci.* **20** 435–42

Weersink R A, Hayward J E, Diamond K R and Patterson M S 1997 Accuracy of noninvasive *in vivo* measurements of photosensitizer uptake based on a diffusion model of reflectance spectroscopy *Photochem. Photobiol.* **66** 326–35

Wolf M, Wolf U, Toronov V, Michalos A, Paunescu L A, Choi J H and Gratton E 2002 Different time evolution of oxyhemoglobin and deoxyhemoglobin concentration changes in the visual and motor cortices during functional stimulation: a near-infrared spectroscopy study *Neuroimage* **16** 704–12

Yaroslavsky I V, Yaroslavsky A N, Schwarzmaier H-J, Akchrin G G and Tuchin V V 1995 New approach to Monte Carlo simulation of photon transport in the frequency-domain *SPIE* **2626** 45–55

Yaroslavsky I V, Yaroslavsky A N, Tuchin V V and Schwarzmaier H-J 1997 Effect of the scattering delay on time-dependent photon migration in turbid media *Appl. Opt.* **36** 6529–38

Zaccanti G 1991 Monte Carlo study of light propagation in optically thick media: point source case *Appl. Opt.* **30** 2031–41